ROYAL SOCIETY
OF CHEMISTRY

PAPER

Check for updates

Copper-doped metal–organic frameworks for the controlled generation of nitric oxide from endogenous *S*-nitrosothiols†

Yingzhu Zhou, [iD] [a] Tao Yang, [iD] [a] Rashin Namivandi-Zangeneh,[ab] Cyrille Boyer, [iD] [ab] Kang Liang [iD] *[ac] and Rona Chandrawati [iD] *[a]

Nitric oxide (NO) is an essential signaling molecule with a number of biological functions and holds great promise in biomedical applications. However, NO delivery technologies have been complicated due to the inherent properties of NO which include short half-life and limited transport distance in human tissues. In addition, the biofunctionality of NO is strongly dependent on its concentrations and locations where it is delivered. To achieve controlled NO delivery, many studies have focused on encapsulating NO donors into macromolecular scaffolds or using catalysts to realize *in situ* NO generation from NO prodrugs. Successful applications have been shown, however NO donor-loaded platforms experience the limitation of finite NO storage capacity. The present study reports the synthesis of a catalyst, copper-doped zeolitic imidazolate framework ZIF-8 (Cu^{2+}/ZIF-8), that is designed to generate NO from naturally occurring endogenous NO donors. By tuning the copper doping percentages, we achieved controlled NO generation from *S*-nitrosoglutathione (GSNO) and *S*-nitrosocysteine (CysNO). Cu^{2+}/ZIF-8 particles retained their catalytic potency after 5 NO generation cycles and we showed that our copper-doped ZIF-8 catalyst produced a 10-fold increased amount of NO compared with previous reports. As a proof-of-concept study, we demonstrated the ability of copper-doped ZIF-8 to disperse bacterial biofilms in the presence of GSNO.

Introduction

Nitric oxide (NO), being recognized as a potent signaling molecule, has been implicated to mediate a collection of physiological processes, such as vasodilation, wound healing, angiogenesis, inflammatory responses, and antimicrobial and tumoricidal activities.[1–5] As a result, an ever-growing interest has focused on developing NO delivery systems for different biomedical applications. Low molecular weight (LMW) NO donors, such as organic nitrates, metal–NO complexes, *S*-nitrosothiols (RSNOs), and diazeniumdiolates (NONOates), are the first-generation of NO delivery platforms reported.[6,7] These donors carry NO moieties and can release them upon activation (*e.g. via* physical stimulation or enzymatic activities).

However, the direct application of LMW NO donors in clinical settings faces the issues of burst release and non-targeted delivery. On this account, the second-generation of NO delivery systems emerged and is constructed by encapsulating NO donors into macromolecular scaffolds, including liposomes, micelles, dendrimers, nanoparticles, and hydrogels.[8–13] These systems have been demonstrated to release NO in a controlled manner to accommodate diverse biomedical applications, however, there exists a challenge to render sustained NO delivery due to the finite NO payloads, and hence they are not practical for long-term utilization. Therefore, alternative systems have been proposed and attested for controlled and sustained NO delivery,[14] that is, to catalyze endogenous NO prodrugs (*i.e.* *S*-nitrosoglutathione (GSNO), *S*-nitrosocysteine (CysNO), and *S*-nitrosoalbumin (AlbSNO)) to achieve *in situ* NO generation using enzyme mimics or catalysts.[15]

The Reynolds group is the first to report that copper-based metal–organic frameworks (Cu-MOFs), namely CuBTC and CuBTTri, were able to catalytically decompose endogenous NO prodrugs to release NO.[16–21] Using CuBTTri as a model, they revealed that the catalytic activities stemmed from the presence of active Cu sites on the surfaces of these particles and only a small fraction (1.3 ± 0.4%) of total copper in these
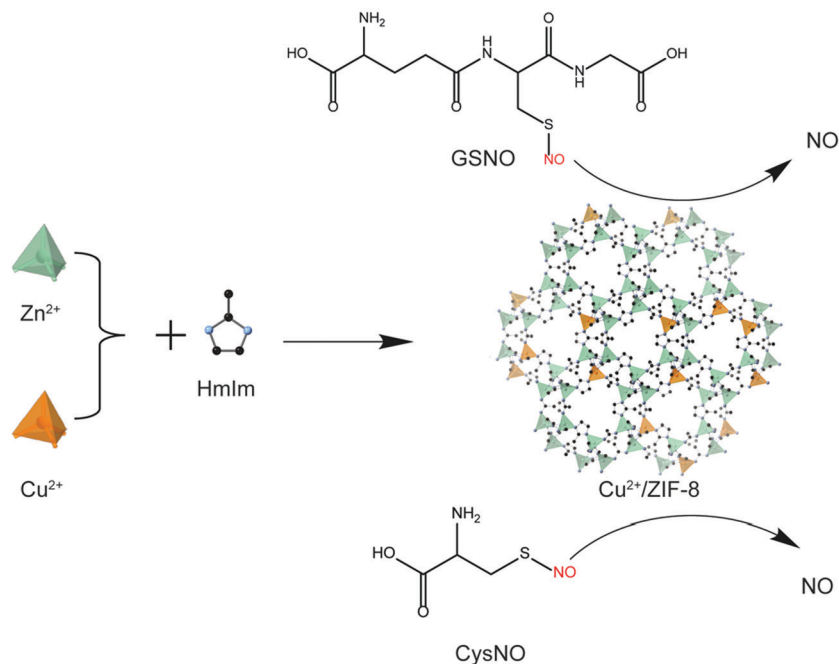
[a] *School of Chemical Engineering and Australian Centre for Nanomedicine (ACN),*
The University of New South Wales (UNSW Sydney), Sydney, NSW 2052, Australia.
E-mail: rona.chandrawati@unsw.edu.au, kang.liang@unsw.edu.au
[b] *Cluster for Advanced Macromolecular Design (CAMD),*
The University of New South Wales (UNSW Sydney), Sydney, NSW 2052, Australia
[c] *Graduate School of Biomedical Engineering, The University of New South Wales*
(UNSW Sydney), Sydney, NSW 2052, Australia
† Electronic supplementary information (ESI) available. See DOI: 10.1039/
d0tb02709j

This journal is © The Royal Society of Chemistry 2021

J. Mater. Chem. B, 2021, **9**, 1059–1068 | **1059**

Scheme 1 Schematic illustration of the synthesis of Cu^{2+}/ZIF-8 which serves as a catalyst for *in situ* NO generation from NO prodrugs, *S*-nitrosoglutathione (GSNO) and *S*-nitrosocysteine (CysNO).

particles was catalytically active.[22] Considering only a minute amount of copper is needed for the NO catalysis reaction, we hypothesize that the remaining non-active copper can be replaced by other more biocompatible metals (*e.g.* Fe, Zn) to reduce the potential risk of copper-induced cytotoxicity.[23–25] Herein, we doped copper ions into zeolitic imidazolate framework (ZIF-8) due to its high biocompatibility, serving as a catalyst for NO delivery. We envision that precisely controlled NO generation can be achieved by simply tuning the copper doping percentages.

In the present study, we: (i) synthesized copper-doped ZIF-8 particles (Cu^{2+}/ZIF-8) and modulated the copper doping percentages by varying the molar ratios between the building blocks; (ii) demonstrated controlled NO release by tuning the concentrations of Cu^{2+}/ZIF-8 particles and NO prodrugs (*i.e.* GSNO and CysNO) (Scheme 1); (iii) examined the catalytic stability of Cu^{2+}/ZIF-8 particles by repeatedly using these particles to catalyze NO prodrugs and comparing the catalytic efficiencies after each cycle; and (iv) illustrated the potential of these particles for antimicrobial applications using an *in vitro* biofilm model.

Materials and methods

Materials

Zinc nitrate hexahydrate ($Zn(NO_3)_2 \cdot 6H_2O$, 98%), 2-methylimidazole (Hmim, 99%), L-cysteine (Cys, ≥98.5%), and hydrochloric acid (HCl) were purchased from Sigma-Aldrich. Copper(II) nitrate trihydrate ($Cu(NO_3)_2 \cdot 3H_2O$, 98.5%), potassium nitrite (KNO_2, ≥96%), sodium phosphate dibasic (Na_2HPO_4), potassium phosphate

monobasic (KH_2PO_4), sodium chloride (NaCl), ammonium chloride (NH_4Cl), magnesium sulfate ($MgSO_4$), calcium chloride ($CaCl_2$), glucose, and absolute methanol were purchased from Chem-Supply. GSNO was purchased from Cayman Chemical. Ultrapure water (18.2 ΩM cm resistance) was provided by arium® mini Sartorius and used throughout the experiments. All reagents were used as received without further purification.

Synthesis of Cu^{2+}/ZIF-8 particles. Cu^{2+}/ZIF-8 particles were synthesized according to the protocol described by Schneider *et al.*[26] Hmim (660 mg in 11.3 mL methanol, 8 mmol) was added dropwise into an equal volume of methanol solution containing 1 mmol of $Zn(NO_3)_2$ and $Cu(NO_3)_2$ using a syringe pump with a flow rate of 0.5 mL s^{-1}. The mixture was allowed to react under constant stirring (400 rpm) at room temperature for 1 h. After reaction, the precipitates were collected by centrifugation (5000 rpm, 5 min) and washed with copious methanol, followed by drying under ambient conditions. By this method, we achieved a 29.56 ± 0.85% yield of Cu^{2+}/ZIF-8. The amount of copper doped was tuned by varying the molar ratio between $Zn(NO_3)_2$ and $Cu(NO_3)_2$ as shown in Table 1. The particles prepared for 0%, 1%, 5%, 10%, and 20% theoretical copper doping percentages will be denoted as ZIF-8, 1% Cu^{2+}/ZIF-8, 5% Cu^{2+}/ZIF-8, 10% Cu^{2+}/ZIF-8, and 20% Cu^{2+}/ZIF-8, respectively.

Characterization of Cu^{2+}/ZIF-8 particles. The crystalline structure of the synthesized particles was confirmed using thin film X-ray diffraction (XRD, PANalytical Empyrean 1 Thin-Film XRD) at 40 kV and 40 mA with a Cu-Kα radiation source. To prepare samples for XRD analysis, 20 μL of highly concentrated particle suspension (in H_2O, 1 mg mL^{-1}) was dropped onto a glass slide, followed by drying at 60 °C for 4 h. The morphology and elemental composition of Cu^{2+}/ZIF-8 particles were

1060 | *J. Mater. Chem. B*, 2021, **9**, 1059–1068

This journal is © The Royal Society of Chemistry 2021

Table 1 The molarities of building blocks used to synthesize ZIF-8 particles with different copper doping percentages

Sample	Theoretical copper doping percentage (%)	Hmim (mmol)	Zn(NO$_3$)$_2$· 6H$_2$O (mmol)	Cu(NO$_3$)$_2$· 3H$_2$O (mmol)
ZIF-8	0	8	1.00	0
1% Cu^{2+}/ZIF-8	1	8	0.99	0.01
5% Cu^{2+}/ZIF-8	5	8	0.95	0.05
10% Cu^{2+}/ZIF-8	10	8	0.90	0.10
20% Cu^{2+}/ZIF-8	20	8	0.80	0.20

characterized by field emission scanning electron microscopy (FESEM, FEI Nova NanoSEM 230) at an acceleration voltage of 5.0 kV and energy dispersive spectroscopy (EDS, Bruker SDD-EDS) respectively. Sample preparation for FESEM imaging and EDS analysis is described as follows. Briefly, 10 µL of 0.1 mg mL^{-1} well-dispersed particle suspension was dropped onto silica wafers and dried at 60 °C overnight. After drying, all samples were coated with a thin layer of platinum (10 nm, for SEM imaging) or carbon (15 nm, for EDS analysis) employing a Leica ACE600 sputter coater and a DCT Desktop carbon evaporator respectively. Platinum coating was introduced to improve the electron signal from the specimen to obtain high signal-to-noise images, while the introduction of carbon coating was to avoid interference with other elements. To determine the actual copper doping ratios, 10 mg of Cu^{2+}/ZIF-8 particles were digested with 1 mL of concentrated nitric acid, followed by dilution with H$_2$O to achieve a final volume of 10 mL. Cu^{2+} concentrations of the obtained clear solutions were measured by inductively coupled plasma optical emission spectroscopy (ICP-OES, PerkinElmer OPTIMA7300).

Synthesis of CysNO. CysNO was synthesized following a previous report by Peterson *et al.*[27] with slight modifications. Briefly, 0.5 mL of 5 mM cysteine was mixed with an equal volume of 5 mM KNO$_2$. Both of the reagents were dissolved in 0.1 M HCl. The reaction was allowed to proceed at room temperature with constant stirring (300 rpm) for 5 min. Light exposure is avoided throughout the experiment. After reaction, more than 90% of cysteine was converted into CysNO.[27] CysNO was freshly prepared before use as it is easy to be oxidized.

Nitric oxide generation. To monitor NO generation from endogenous *S*-nitrosothiols in real time, a free radical analyzer (TBR4100, World Precision Instrument) equipped with an NO sensitive probe (ISO-NOP, World Precision Instrument) was employed. TBR 4100 measures NO kinetics using the amperometric detection principle, that is, changes in current are recorded and converted into NO concentrations based on a calibration curve. In detail, the ISO-NOP sensor was first polarized overnight, then calibrated by adding 25 µM KNO$_2$ in 10 mL of 0.1 M H$_2$SO$_4$ + 0.1 M KI solution at 37 °C. At least five proportional increasing volumes of KNO$_2$ were added each time after a stable current baseline was obtained. The calibration curve was derived based on 1:1 NO generation by different amounts of KNO$_2$ added. To follow the NO generation profiles of RSNOs, the NO electrode was firstly immersed into 3.95 mL particle suspensions (0.01–0.1 mg mL^{-1}) in 10 mM PBS for 1 h at

37 °C. Then, when the system reached a stable baseline, 50 µL of RSNO (*i.e.* GSNO or CysNO) solutions were added into the suspensions to achieve a final concentration of 1–50 µM. The changes in current were monitored over time and the entire reaction was conducted at 37 °C in dark under constant stirring (400 rpm).

Catalytic stability of Cu^{2+}/ZIF-8 particles. The catalytic stability of Cu^{2+}/ZIF-8 particles to generate NO was evaluated using a free radical analyzer. In brief, the NO-sensitive electrode was immersed into 3.95 mL Cu^{2+}/ZIF-8 suspensions (0.1 mg mL^{-1}). 50 µL GSNO solutions (50 µM) were then added into the particle suspension and changes in current were recorded over time. This process was repeated 5 times when the current signals decayed back to a stable baseline. The whole experiment was conducted at 37 °C in dark under constant stirring (400 rpm). The catalytic efficiency was calculated based on the following equation:

$$\% \text{ catalytic efficiency} = \frac{A_i}{A_0} \times 100$$

where A_0 is the peak NO concentration generated from the first GSNO dosage, A_i is the peak NO concentration generated from the following cycles (i = 2nd, 3rd, 4th, and 5th cycles).

Biofilm dispersal study. The laboratory strain *Pseudomonas aeruginosa* PAO1 was used to grow biofilm. In all assays, a single colony of PAO1 was inoculated in 10 mL of Luria Bertani medium (LB 10) at 37 °C with shaking at 180 rpm overnight. The overnight culture was diluted 1:200 in freshly prepared M9 minimal medium containing 48 mM Na$_2$HPO$_4$, 22 mM KH$_2$PO$_4$, 9 mM NaCl, 19 mM NH$_4$Cl, pH 7.0, supplemented with 2 mM MgSO$_4$, 100 µM CaCl$_2$ and 20 mM glucose. The bacterial suspension was then aliquoted 1 mL per well of tissue-culture treated 24-well plates (Costar, Corning®). The plates were incubated at 37 °C with shaking at 180 rpm in an orbital shaker (model OM11, Ratek, Australia) and the biofilm cultures were allowed to grow for 6.5 h. To characterize the effect of catalytic and controlled NO generation of Cu^{2+}/ZIF-8 on the biofilm dispersal, preformed PAO1 biofilms were treated with Cu^{2+}/ZIF-8 particles in the presence or absence of GSNO and incubated for 30 min. Biofilm biomass was quantified using the crystal violet (CV) staining method. Briefly, after treatment, the culture supernatant was removed and the biofilm on the well surfaces was washed once with 1 mL of PBS, followed by the addition of 1 mL 0.03% CV stain made from a 1:10 dilution of CV (BD) in PBS. The plates were incubated on the bench for 20 min before the wells were washed twice with PBS. The CV stained biofilms were mixed with 1 mL 100% ethanol and the biofilm biomass was quantified by measuring the OD$_{595}$ of the homogenized suspension using a microtiter plate reader (FLUOstar Omega, BMG Labtech). The biofilm dispersal was calculated by the following equation:

$$\% \text{ biofilm dispersal} = \frac{A_p - A_s}{A_p} \times 100$$

where A_p is the absorbance of control without particles or GSNO, A_s is the absorbance of the tested samples. All assays
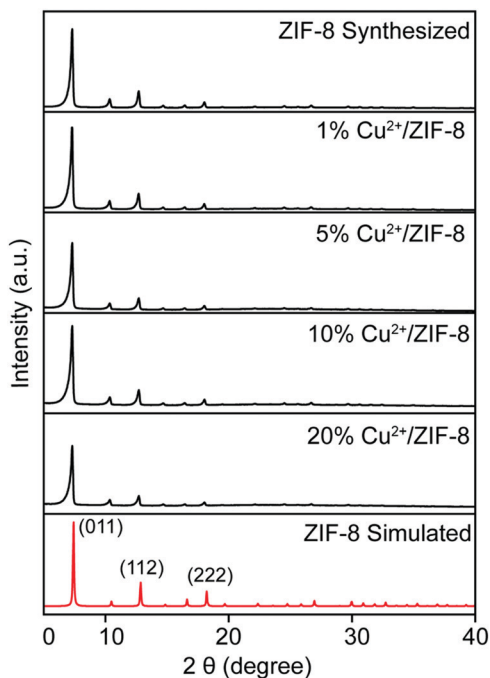
Fig. 1 XRD patterns of ZIF-8 and 1%, 5%, 10%, and 20% Cu^{2+}/ZIF-8.

included two replicates and were repeated in three independent experiments.

Results and discussion

Characterization of Cu^{2+}/ZIF-8

Cu^{2+}/ZIF-8 particles were synthesized by reacting $Cu(NO_3)_2$, $Zn(NO_3)_2$, and 2-methylimidazole in methanol. The theoretical levels (0, 1, 5, 10, and 20%) of copper doping were tuned by varying the molar ratio between $Cu(NO_3)_2$ and $Zn(NO_3)_2$. All types of particles were firstly analyzed using XRD to confirm their crystalline structures. As shown in Fig. 1, all samples display characteristic peaks of (011), (112), and (222) which can be indexed to the noncentrosymmetric cubic ZIF-8 pattern (space group $I\bar{4}3m$; $a_0 = 16.9910$ Å, $V = 4905.2$ Å^3 [28]). In addition, all particles exhibit high crystallinity as evidenced by the sharp peaks. These suggest that copper doping did not compromise the crystal structure of the host material, in this case, ZIF-8. The next step, we characterized all particles using ICP-OES to determine the actual amount of copper ions doped. As shown in Table 2, the final copper loadings in Cu^{2+}/ZIF-8 particles are $0.08 \pm 0.00\%$, $0.28 \pm 0.04\%$, $0.47 \pm 0.05\%$, and $0.76 \pm 0.06\%$ for reactions performed in the presence of 1, 5, 10, and 20% $Cu(NO_3)_2$ respectively. The actual doping percentages are lower than the theoretical values, which is consistent with the previous studies. [29–31]

ICP-OES reveals the presence of Cu^{2+} ions in ZIF-8 particles with controllable copper levels. To further support this conclusion, all particles were characterized using energy-dispersive
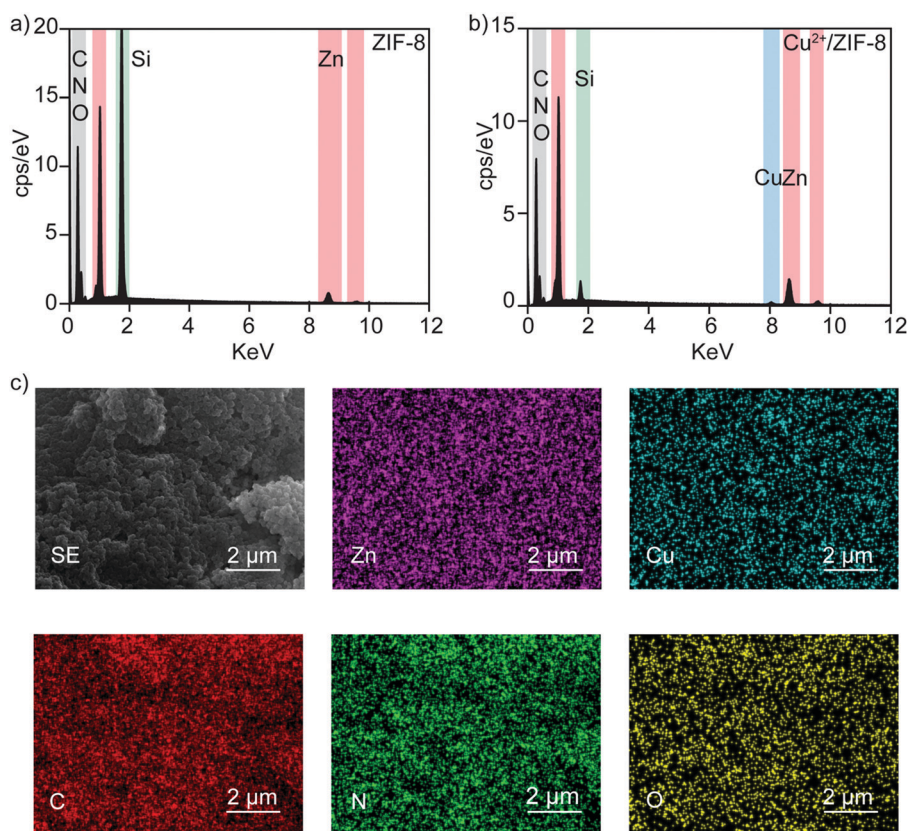

Fig. 2 EDS spectra of (a) ZIF-8 and (b) 20% Cu^{2+}/ZIF-8. (c) Elemental mapping of 20% Cu^{2+}/ZIF-8. Images shown are secondary electron (SE) image, elemental distribution of zinc (pink), copper (blue), carbon (red), nitrogen (green), and oxygen (yellow).

Table 2 Theoretical and actual copper doping and zinc percentages in each sample. The as-synthesized particles were washed and dried (to remove any excess and free copper ions) prior to digestion with concentrated nitric acid for ICP-OES analysis

Sample	Theoretical copper doping percentage (%)	Actual copper doping percentage (%)	Actual zinc percentage (%)
ZIF-8	0	0.00 ± 0.00	12.70 ± 0.27
1% Cu^{2+}/ZIF-8	1	0.08 ± 0.00	13.10 ± 0.73
5% Cu^{2+}/ZIF-8	5	0.28 ± 0.04	12.89 ± 0.70
10% Cu^{2+}/ZIF-8	10	0.47 ± 0.05	12.83 ± 0.67
20% Cu^{2+}/ZIF-8	20	0.76 ± 0.06	12.96 ± 0.76

X-ray spectroscopy to identify their elemental composition. Fig. 2a and b show the EDS spectra of pristine ZIF-8 and 20% Cu^{2+}/ZIF-8 particles, respectively. Besides the characteristic peaks of Zn positioned at 8.6 and 9.6 keV, an additional Cu peak at 8.0 keV was observed for 20% Cu^{2+}/ZIF-8 particles, indicating successful copper inclusion. The detected C and N peaks were generated from organic linkers, O peaks from residual NO_3^- from the metal salts, and Si peaks from silica wafers. Furthermore, elemental mapping using SEM for the 20% Cu^{2+}/ZIF-8 particles showed that Zn and Cu elements were uniformly distributed (Fig. 2c).

SEM analysis was performed to investigate the morphology of the particles synthesized. Regardless of the doping percentages, all types of particles exhibited the typical rhombic dodecahedron morphology of ZIF-8 particles[32] (Fig. 3a–i), implicating that the influence of copper doping on the microstructures of the host ZIF-8 particles is negligible. Particle sizes were measured using ImageJ software from the SEM images recorded and the particle size distribution was determined using Origin software (Gaussian fitting). As shown in Fig. 3b–j, compared to pristine ZIF-8 particles (87.3 ± 7.8 nm), the average diameters for particles with copper doping are 103.6 ± 11.2 nm for 1% Cu^{2+}/ZIF-8, 112.3 ± 9.4 nm for 5% Cu^{2+}/ZIF-8, 119.4 ± 9.6 nm for 10% Cu^{2+}/ZIF-8, with a slight increase in particle size observed for 20% Cu^{2+}/ZIF-8 (139.9 ± 14.0 nm).

Controlled NO generation by Cu^{2+}/ZIF-8 particles

It has been well studied that copper ions can catalyze RSNOs to release NO through the copper-catalyzed S–N bond cleavage in GSNO.[33–35] Therefore, in the next step, we examined the ability of Cu^{2+}/ZIF-8 particles to decompose GSNO, a commercially available endogenous NO prodrug, to release NO. A NO-sensitive electrochemical probe with a detection limit of 1 nM was utilized to monitor the NO release profiles in real time. In our experiments, the NO probe was immersed and equilibrated in suspensions of ZIF-8 particles with different copper doping levels (pH 7.4, 37 °C), followed by the administration of 50 μM GSNO. NO release kinetics was monitored over time using the associated LabScribe2 software. As shown in Fig. 4a, NO generation was observed for ZIF-8 particles with higher copper doping ratios and NO peaked at concentrations of 1.01 ± 0.01 μM (5%), 1.51 ± 0.01 μM (10%), and 2.99 ± 0.03 μM (20%). The peak NO levels for pristine ZIF-8 (0.49 ± 0.03 μM) and 1% Cu^{2+}/ZIF-8
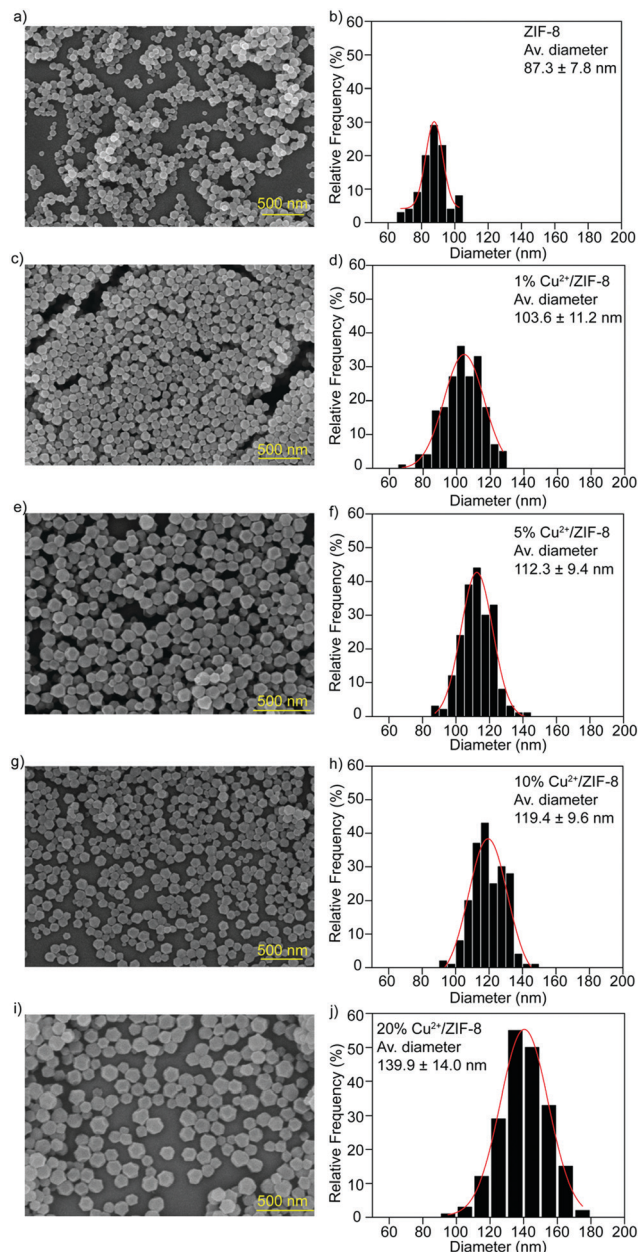

Fig. 3 SEM images and size distributions of (a and b) ZIF-8, (c and d) 1% Cu^{2+}/ZIF-8, (e and f) 5% Cu^{2+}/ZIF-8, (g and h) 10% Cu^{2+}/ZIF-8, and (i and j) 20% Cu^{2+}/ZIF-8. Scale bars: 500 nm.

(0.66 ± 0.02 μM) particles are comparable to that of GSNO alone (0.49 ± 0.02 μM), indicating a doping level of 5% and higher is required to promote GSNO decomposition. The NO peak observed for GSNO only is possibly attributed to GSNO self-decomposition as shown by previous studies.[36–38] Peak NO concentrations and copper doping percentages exhibited a linear relationship ($R^2 = 0.97$) (Fig. 4b). Owing to its highest catalytic efficacy, 20% Cu^{2+}/ZIF-8 particles were selected for the following experiments. To demonstrate tunable and controlled NO generation, NO release from GSNO solutions at a wide range of concentrations (1–50 μM) was measured in the presence of 0.1 mg mL^{-1} of 20% Cu^{2+}/ZIF-8 particles.
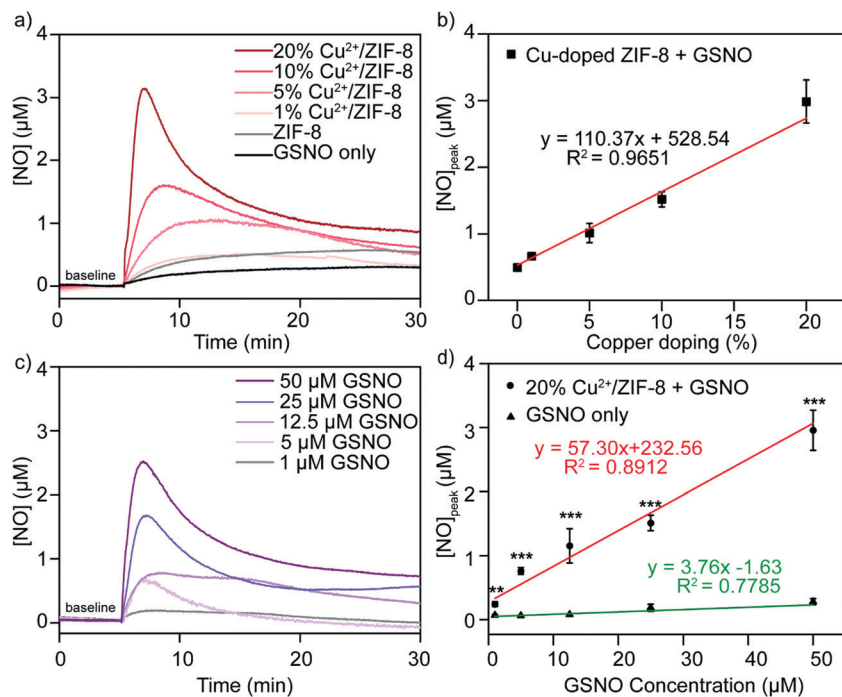
Fig. 4 (a) Representative NO generation profiles and (b) peak NO concentrations from GSNO (50 μM) in the presence of Cu^{2+}/ZIF-8 (0.1 mg mL^{-1}) with different copper doping percentages (0–20%). (c) Representative NO generation profiles and (d) peak NO concentrations from catalytic decomposition of GSNO (1–50 μM) by 20% Cu^{2+}/ZIF-8 (0.1 mg mL^{-1}). All reactions were performed in PBS at 37 °C. Values represent mean ± standard deviation, $n = 3$. Statistical significance relative to control tests was calculated, $**p < 0.01$, $***p < 0.001$ (one-way ANOVA followed by Tukey *post hoc* test).
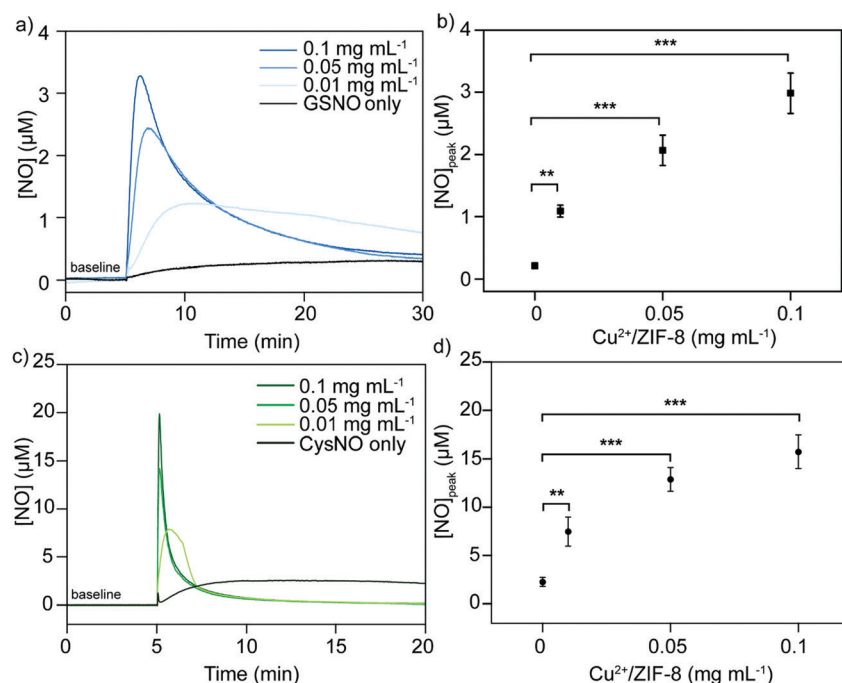

Fig. 5 (a) Representative NO generation curves and (b) peak NO concentrations from GSNO (50 μM) by 20% Cu^{2+}/ZIF-8 (0.01–0.1 mg mL^{-1}). (c) Representative NO generation curves and (b) peak NO concentrations from CysNO (50 μM) by 20% Cu^{2+}/ZIF-8 (0.01–0.1 mg mL^{-1}). Values represent mean ± standard deviation, $n = 3$. Statistical significance relative to control tests was calculated, $**p < 0.01$, $*** p < 0.001$ (one-way ANOVA followed by Tukey *post hoc* test).
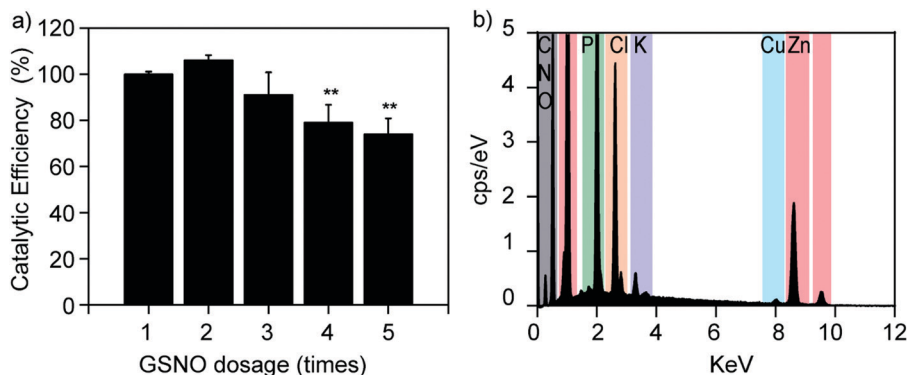
Fig. 6 (a) Catalytic efficiencies of 20% Cu^{2+}/ZIF-8 particles (0.1 mg mL^{-1}) after continuous addition of GSNO solutions (50 μM). Values represent mean ± standard deviation, n = 3. Statistical significance relative to the first dosage was calculated, **p < 0.01 (one-way ANOVA followed by Tukey *post hoc* test). (b) EDS spectrum of 20% Cu^{2+}/ZIF-8 after reaction with GSNO.

As expected, we observed a dose-dependent NO generation from GSNO (Fig. 4c and d), that is, NO levels peaked at 0.20 ± 0.04 μM, 0.73 ± 0.06 μM, 1.14 ± 0.28 μM, 1.50 ± 0.13 μM, and 2.99 ± 0.32 μM for 1, 5, 12.5, 25, and 50 μM GSNO, respectively. Compared with previous studies that demonstrated the generation of NO with peak concentrations of ∼0.1 μM in the presence of CuBTTri and 20 μM GSNO,[20,21] copper-doped ZIF-8 particles reported in this work produce a 10-fold increase in NO generation. It is important to note that NO release measurements in the previous studies were performed using a chemiluminescence-based NO analyzer, while in this work we used an electrochemical method.[39,40]

Alternatively, we varied the concentrations of 20% Cu^{2+}/ZIF-8 from 0.01 to 0.1 mg mL^{-1} while maintaining the level of GSNO at 50 μM (Fig. 5a). Surprisingly, a surge of 1.09 ± 0.10 μM NO was generated even though only 0.01 mg mL^{-1} Cu^{2+}/ZIF-8 particles were used, indicating the strong catalytic efficiency of these particles towards GSNO (Fig. 5b). When 0.05 and 0.1 mg mL^{-1} of Cu^{2+}/ZIF-8 particles were utilized, the amount of NO produced was 2.07 ± 0.24 μM and 2.99 ± 0.32 μM respectively.

Following the same experimental procedures, the NO-generating activity of Cu^{2+}/ZIF-8 was also examined against another class of endogenous NO prodrugs, CysNO. On the one hand, we found that higher NO levels were achieved from CysNO as the concentrations of Cu^{2+}/ZIF-8 increased (Fig. 5c and d). On the other hand, at the same catalyst concentration, a significantly higher decomposition rate was observed for CysNO compared to GSNO. For instance, the peak NO concentrations for CysNO were 7.47 ± 1.50 μM, 12.88 ± 1.23 μM, and 15.73 ± 1.73 μM in the presence of 0.01, 0.05, and 0.1 mg mL^{-1} Cu^{2+}/ZIF-8 respectively, which is ∼6 times higher than those of GSNO. This attribute shows that GSNO is more stable than CysNO and it is easier to decompose the latter using Cu^{2+}/ZIF-8 under physiological conditions (pH = 7.4, 37 °C).[41,42]

Catalytic stability of Cu^{2+}/ZIF-8 particles

The catalytic stability of Cu^{2+}/ZIF-8 particles is of great importance, especially for long-term applications. To investigate this, we repeatedly spiked 50 μM GSNO solutions into the same Cu^{2+}/ZIF-8 suspension and compared the catalytic efficiencies after each addition. As shown in Fig. 6a, Cu^{2+}/ZIF-8 particles retained 100% and 75% of their original catalytic potency after 2 and 5 cycles respectively, confirming that their biocatalytic performance can be well-maintained suitable for repeated use. Our results are comparable to those reported by Reynolds *et al.* In their study, a water-soluble Cu-MOF (CuBTTri) was embedded into chitosan to formulate NO-generating films. The catalytic efficiencies of these films towards GSNO were completely preserved after 4 cycles of reuse.[20] In addition, to investigate the stability of copper ions in Cu^{2+}/ZIF-8, we performed EDS analysis on 20% Cu^{2+}/ZIF-8 particles after reaction with GSNO. In brief, 20% Cu^{2+}/ZIF-8 particles were suspended in PBS, followed by the addition of 50 μM GSNO. After 24 h incubation at 37 °C, the particles were collected by centrifugation and EDS analysis was performed. As shown in Fig. 6b, we observed a clear Cu peak at 8.0 keV, indicating there was no noticeable copper leakage during the timeframe we investigated. The additional P, Cl, and K peaks originated from residuals of PBS buffer. Furthermore, we investigated the morphology of 20% Cu^{2+}/ZIF-8 particles after the reaction with GSNO. We observed that the particles changed their morphology from the pristine rhombic dodecahedron shape to a less regular form (Fig. S1, ESI†), similar to morphology changes of ZIF-8 described in previous publications.[43,44] It is worth noting that Cu^{2+}/ZIF-8 particles maintained their catalytic capacity for NO generation after 5 cycles of reuse as shown in Fig. 6a, indicating the morphological transformation plays a minor effect on the catalytic stability of these particles.

Biofilm dispersal activities of Cu^{2+}/ZIF-8 particles

As illustrated above, by tuning the concentrations of Cu^{2+}/ZIF-8 particles and NO prodrugs, we could achieve μM levels of NO at which NO has been proven to exhibit antimicrobial activity.[45,46] Therefore, in the following experiments, we aim to demonstrate the potential of Cu^{2+}/ZIF-8 particles for antimicrobial application (*i.e.* to disperse biofilms). *P. aeruginosa* is a Gram-negative bacterium that contributes to an estimated 10–20% of all hospital-acquired infections[47] and hence is selected for our studies. Preformed *P. aeruginosa* biofilms were incubated
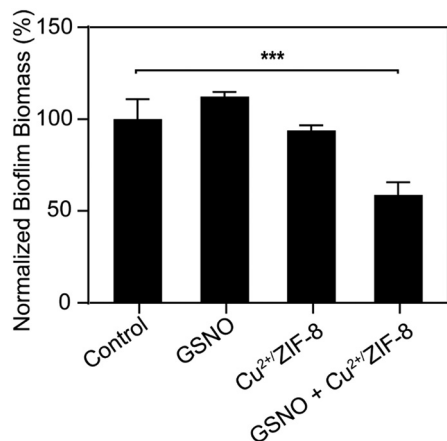
Fig. 7 The ability of 20% Cu^{2+}/ZIF-8 particles (0.3 mg mL^{-1}) to disperse *P. aeruginosa* biofilms in the presence of 1 mM GSNO. All values are normalized to the biofilm biomass without GSNO or Cu^{2+}/ZIF-8 treatment (control). Values represent mean ± standard deviation, $n = 3$. Statistical significance relative to control tests was calculated, ***$p < 0.001$ (one-way ANOVA followed by Tukey *post hoc* test).

with Cu^{2+}/ZIF-8 particles in the presence or absence of GSNO and the remaining biomass of the biofilms was measured using crystal violet assay. As shown in Fig. 7, there was no noticeable reduction in biomass for biofilms solely treated with Cu^{2+}/ZIF-8 (0.3 mg mL^{-1}) or GSNO (1 mM). On the other hand, the administration of both components (Cu^{2+}/ZIF-8 and GSNO) led to a 45% reduction in the biomass of *P. aeruginosa* biofilms, indicating the essential role of Cu^{2+}/ZIF-8 particles to catalyze GSNO for NO generation and hence to exert antibiofilm activity.

Conclusions

In conclusion, we reported a catalyst, namely Cu^{2+}/ZIF-8 particles, for controlled NO generation. NO levels of biologically relevant can be achieved by tuning the copper doping percentages and varying the concentrations of Cu^{2+}/ZIF-8 particles and RSNOs. Cu^{2+}/ZIF-8 maintained 75% of its original catalytic efficiency after 5 cycles of NO generation, indicating their potential for long-term biomedical use. Using a *P. aeruginosa* biofilm model, we observed that the co-administration of Cu^{2+}/ZIF-8 particles and GSNO resulted in a 45% reduction in biofilm biomass, making these particles candidates for antimicrobial applications. Future studies may focus on designing multifunctional catalysts using Cu^{2+}/ZIF-8 particles as a template, specifically, to load enzymes/drugs into ZIF-8 to take advantage of their high surface areas.

Conflicts of interest

There are no conflicts of interest to declare.

Acknowledgements

References

1 R. Zamora, Y. Vodovotz and T. R. Billiar, Inducible nitric oxide synthase and inflammatory diseases, *Mol. Med.*, 2000, **6**(5), 347.

2 M. R. Schäffer, U. Tantry, S. S. Gross, H. L. Wasserkrug and A. Barbul, Nitric oxide regulates wound healing, *J. Surg. Res.*, 1996, **63**(1), 237–240.

3 L. Yang, E. S. Feura, M. J. R. Ahonen and M. H. Schoenfisch, Nitric oxide-releasing macromolecular scaffolds for antibacterial applications, *Adv. Healthcare Mater.*, 2018, **7**(13), 1800155.

4 P. Lala, Significance of nitric oxide in carcinogenesis, tumor progression and cancer therapy, *Cancer Metastasis Rev.*, 1998, **17**(1), 1.

5 A. K. Winther, B. Fejerskov, M. ter Meer, N. B. S. Jensen, R. Dillion, J. E. Schaffer, R. Chandrawati, M. M. Stevens, L. J. Schultze Kool, U. Simonsen and A. N. Zelikin, Enzyme prodrug therapy achieves site-specific, personalized physiological responses to the locally produced nitric oxide, *ACS Appl. Mater. Interfaces*, 2018, **10**(13), 10741–10751.

6 E. van Faassen and A. F. Vanin, Low-molecular-weight S-nitrosothiols, in *Radicals for Life*, Elsevier, 2007, pp. 173–199.

7 A.-S. D. Haitham and A. J. C. s. Ferro, S-Nitrosothiols: a class of nitric oxide-donor drugs, *Clin. Sci.*, 2000, **98**(5), 507–520.

8 Y. Wo, E. J. Brisbois, R. H. Bartlett and M. E. Meyerhoff, Recent advances in thromboresistant and antimicrobial polymers for biomedical applications: just say yes to nitric oxide (NO), *Biomater. Sci.*, 2016, **4**(8), 1161–1183.

9 T. Yang, A. N. Zelikin and R. Chandrawati, Progress and promise of nitric oxide-releasing platforms, *Adv. Sci.*, 2018, **5**(6), 1701043.

10 R. Chandrawati, J. Y. Chang, E. Reina-Torres, C. Jumeaux, J. M. Sherwood, W. D. Stamer, A. N. Zelikin, D. R. Overby and M. M. Stevens, Localized and controlled delivery of nitric oxide to the conventional outflow pathway via enzyme biocatalysis: toward therapy for glaucoma, *Adv. Mater.*, 2017, **29**(16), 1604932.

11 Z. Sadrearhami, T.-K. Nguyen, R. Namivandi-Zangeneh, K. Jung, E. H. Wong and C. Boyer, Recent advances in nitric oxide delivery for antimicrobial applications using polymer-based systems, *J. Mater. Chem. B*, 2018, **6**(19), 2945–2959.

12 H. T. T. Duong, K. Jung, S. K. Kutty, S. Agustina, N. N. M. Adnan, J. S. Basuki, N. Kumar, T. P. Davis, N. Barraud and C. Boyer, Nanoparticle (star polymer) delivery of nitric oxide effectively negates *Pseudomonas aeruginosa* biofilm formation, *Biomacromolecules*, 2014, **15**(7), 2583–2589.

1066 | *J. Mater. Chem. B*, 2021, **9**, 1059–1068

This journal is © The Royal Society of Chemistry 2021

13 T.-K. Nguyen, R. Selvanayagam, K. K. K. Ho, R. Chen, S. K. Kutty, S. A. Rice, N. Kumar, N. Barraud, H. T. T. Duong and C. Boyer, Co-delivery of nitric oxide and antibiotic using polymeric nanoparticles, *Chem. Sci.*, 2016, **7**(2), 1016–1027.

14 T. Yang, A. N. Zelikin and R. Chandrawati, Enzyme mimics for the catalytic generation of nitric oxide from endogenous prodrugs, *Small*, 2020, **16**, 1907635.

15 T. Yang, A. S. Fruergaard, A. K. Winther, A. N. Zelikin and R. Chandrawati, Zinc oxide particles catalytically generate nitric oxide from endogenous and exogenous prodrugs, *Small*, 2020, **16**, 1906744.

16 J. L. Harding and M. M. Reynolds, Metal organic frameworks as nitric oxide catalysts, *J. Am. Chem. Soc.*, 2012, **134**(7), 3330–3333.

17 J. L. Harding and M. M. Reynolds, Composite materials with embedded metal organic framework catalysts for nitric oxide release from bioavailable *S*-nitrosothiols, *J. Mater. Chem. B*, 2014, **2**(17), 2530–2536.

18 J. L. Harding, J. M. Metz and M. M. Reynolds, A tunable, stable, and bioactive MOF catalyst for generating a localized therapeutic from endogenous sources, *Adv. Funct. Mater.*, 2014, **24**(47), 7503–7509.

19 M. J. Neufeld, B. R. Ware, A. Lutzke, S. R. Khetani and M. M. Reynolds, Water-stable metal–organic framework/polymer composites compatible with human hepatocytes, *ACS Appl. Mater. Interfaces*, 2016, **8**(30), 19343–19352.

20 M. J. Neufeld, A. Lutzke, J. B. Tapia and M. M. Reynolds, Metal–organic framework/chitosan hybrid materials promote nitric oxide release from *S*-nitrosoglutathione in aqueous solution, *ACS Appl. Mater. Interfaces*, 2017, **9**(6), 5139–5148.

21 M. J. Neufeld, A. Lutzke, W. M. Jones and M. M. Reynolds, Nitric oxide generation from endogenous substrates using metal–organic frameworks: inclusion within poly(vinyl alcohol) membranes to investigate reactivity and therapeutic potential, *ACS Appl. Mater. Interfaces*, 2017, **9**(41), 35628–35641.

22 R. R. Tuttle, S. J. Folkman, H. N. Rubin, R. G. Finke and M. M. Reynolds, Copper metal–organic framework surface catalysis: catalyst poisoning, IR spectroscopic, and kinetic evidence addressing the nature and number of the catalytically active sites en route to improved applications, *ACS Appl. Mater. Interfaces*, 2020, **12**(35), 39043–39055.

23 N. Hanagata, F. Zhuang, S. Connolly, J. Li, N. Ogawa and M. Xu, Molecular responses of human lung epithelial cells to the toxicity of copper oxide nanoparticles inferred from whole genome expression analysis, *ACS Nano*, 2011, **5**(12), 9326–9338.

24 Z. Chen, H. Meng, G. Xing, C. Chen, Y. Zhao, G. Jia, T. Wang, H. Yuan, C. Ye and F. Zhao, Acute toxicological effects of copper nanoparticles *in vivo*, *Toxicol. Lett.*, 2006, **163**(2), 109–120.

25 K. Jomova and M. Valko, Advances in metal-induced oxidative stress and human disease, *Toxicology*, 2011, **283**(2–3), 65–87.

26 A. Schejn, A. Aboulaich, L. Balan, V. Falk, J. Lalevée, G. Medjahdi, L. Aranda, K. Mozet and R. J. C. S. Schneider, Technology, Cu^{2+}-doped zeolitic imidazolate frameworks (ZIF-8): efficient and stable catalysts for cycloadditions and condensation reactions, *Catal. Sci. Technol.*, 2015, **5**(3), 1829–1839.

27 L. A. Peterson, T. Wagener, H. Sies and W. J. C. Stahl, r. i. t., Decomposition of *S*-nitrosocysteine via *S*- to *N*-transnitrosation, *Chem. Res. Toxicol.*, 2007, **20**(5), 721–723.

28 K. S. Park, Z. Ni, A. P. Cote, J. Y. Choi, R. D. Huang, F. J. Uribe-Romo, H. K. Chae, M. O'Keeffe and O. M. Yaghi, Exceptional chemical and thermal stability of zeolitic imidazolate frameworks, *Proc. Natl. Acad. Sci. U. S. A.*, 2006, **103**(27), 10186–10191.

29 N. Nagarjun and A. Dhakshinamoorthy, A Cu-Doped ZIF-8 metal organic framework as a heterogeneous solid catalyst for aerobic oxidation of benzylic hydrocarbons, *New J. Chem.*, 2019, **43**(47), 18702–18712.

30 S. Sun, Z. Yang, J. Cao, Y. Wang and W. Xiong, Copper-doped ZIF-8 with high adsorption performance for removal of tetracycline from aqueous solution, *J. Solid State Chem.*, 2020, **285**, 121219.

31 A. Parkash, Copper doped zeolitic imidazole frameworks (ZIF-8): a new generation of single-atom catalyst for oxygen reduction reaction in alkaline media, *J. Electrochem. Soc.*, 2020, **167**(15), 155504.

32 J. Cravillon, C. A. Schröder, H. Bux, A. Rothkirch, J. Caro and M. Wiebcke, Formate modulated solvothermal synthesis of ZIF-8 investigated using time-resolved *in situ* X-ray diffraction and scanning electron microscopy, *CrystEngComm*, 2012, **14**(2), 492–498.

33 A. C. Gorren, A. Schrammel, K. Schmidt and B. Mayer, Decomposition of *S*-nitrosoglutathione in the presence of copper ions and glutathione, *Arch. Biochem. Biophys.*, 1996, **330**(2), 219–228.

34 J. N. Smith and T. P. Dasgupta, Kinetics and mechanism of the decomposition of *S*-nitrosoglutathione by L-ascorbic acid and copper ions in aqueous solution to produce nitric oxide, *Nitric Oxide*, 2000, **4**(1), 57–66.

35 S. C. Askew, D. J. Barnett, J. McAninly and D. L. H. Williams, Catalysis by Cu^{2+} of nitric oxide release from *S*-nitrosothiols (RSNO), *J. Chem. Soc., Perkin Trans. 2*, 1995, 741–745.

36 G. F. P. de Souza, J. P. Denadai, G. F. Picheth and M. G. de Oliveira, Long-term decomposition of aqueous *S*-nitrosoglutathione and *S*-nitroso-*N*-acetylcysteine: influence of concentration, temperature, pH and light, *Nitric Oxide*, 2019, **84**, 30–37.

37 L. Heikal, G. P. Martin and L. A. Dailey, Characterisation of the decomposition behaviour of *S*-nitrosoglutathione and a new class of analogues: *S*-nitrosophytochelatins, *Nitric Oxide*, 2009, **20**(3), 157–165.

38 J. S. Stamler and E. J. Toone, The decomposition of thionitrites, *Curr. Opin. Chem. Biol.*, 2002, **6**(6), 779–785.

39 P. N. Coneski and M. H. Schoenfisch, Nitric oxide release: part III. Measurement and reporting, *Chem. Soc. Rev.*, 2012, **41**(10), 3753–3758.

This journal is © The Royal Society of Chemistry 2021

J. Mater. Chem. B, 2021, **9**, 1059–1068 | **1067**

40 M. D. Brown and M. H. Schoenfisch, Electrochemical nitric oxide sensors: principles of design and characterization, *Chem. Rev.*, 2019, **119**(22), 11551–11575.

41 J. Gu and R. S. Lewis, Effect of pH and metal ions on the decomposition rate of *S*-nitrosocysteine, *Ann. Biomed. Eng.*, 2007, **35**(9), 1554–1560.

42 M. J. B. e. B. A.-B. Kelm, Nitric oxide metabolism and breakdown, *Biochim. Biophys. Acta, Bioenerg.*, 1999, **1411**(2–3), 273–289.

43 M. d. J. Velásquez-Hernández, R. Ricco, F. Carraro, F. T. Limpoco, M. Linares-Moreau, E. Leitner, H. Wiltsche, J. Rattenberger, H. Schröttner and P. Frühwirt, Degradation of ZIF-8 in phosphate buffered saline media, *CrystEng-Comm*, 2019, **21**(31), 4538–4544.

44 M. A. Luzuriaga, C. E. Benjamin, M. W. Gaertner, H. Lee, F. C. Herbert, S. Mallick and J. J. Gassensmith, ZIF-8 degrades in cell media, serum, and some—but not all—common laboratory buffers, *Supramol. Chem.*, 2019, **31**(8), 485–490.

45 R. Namivandi-Zangeneh, Z. Sadrearhami, A. Bagheri, M. Sauvage-Nguyen, K. K. K. Ho, N. Kumar, E. H. H. Wong and C. Boyer, Nitric oxide-loaded antimicrobial polymer for the synergistic eradication of bacterial biofilm, *ACS Macro Lett.*, 2018, **7**(5), 592–597.

46 D. O. Schairer, J. S. Chouake, J. D. Nosanchuk and A. J. Friedman, The potential of nitric oxide releasing therapies as antimicrobial agents, *Virulence*, 2012, **3**(3), 271–279.

47 V. E. Wagner and B. H. Iglewski, *P. aeruginosa* biofilms in CF infection, *Clin. Rev. Allergy Immunol.*, 2008, **35**(3), 124–134.

1068 | *J. Mater. Chem. B*, 2021, **9**, 1059–1068

This journal is © The Royal Society of Chemistry 2021